ASTM INTERNATIONAL

Geotechnical Testing Journal

Changfu Chen,[1] Genbao Zhang,[1] Jorge Gabriel Zornberg,[2] and Xinxiu Zheng[1]

DOI: 10.1520/GTJ20170431

Element Nail Pullout Tests for Prediction of Soil Nail Pullout Resistance in Expansive Clays

Geotechnical Testing Journal

doi:10.1520/GTJ20170431 available online at www.astm.org

Changfu Chen,[1] Genbao Zhang,[1] Jorge Gabriel Zornberg,[2] and Xinxiu Zheng[1]

Element Nail Pullout Tests for Prediction of Soil Nail Pullout Resistance in Expansive Clays

Reference

Chen, C., Zhang, G., Zornberg, J. G., and Zheng, X., "Element Nail Pullout Tests for Prediction of Soil Nail Pullout Resistance in Expansive Clays," *Geotechnical Testing Journal* https://doi.org/10.1520/GTJ20170431. ISSN 0149-6115

ABSTRACT

The performance of soil nail systems relies primarily on soil-nail interaction, which is especially complex for nails embedded in clay materials. Soil-nail interaction is difficult to predict in these soils because of the effect of moisture-induced stress and swelling along the interface between soil and nail. As part of this investigation, tests were conducted to characterize the soil-nail interface shearing mechanisms using a novel element nail pullout device that involves comparatively short nails embedded in soils under varying degrees of saturation. Additionally, a large-scale pullout test, involving inundation and loading phases, was conducted using soil nails embedded in expansive clays. The soil-nail interface shearing mechanisms identified with the element nail pullout device and the vertical rise measurements of the clay from the inundation test were used within a load transfer theoretical framework aimed at predicting the response of soil nails in expansive clays. This load transfer framework provided a very good prediction of the large-scale pullout test results using the data collected from the element nail pullout tests.

Keywords

soil nailing, element test, interface shear strength, vertical rise, load transfer, expansive clays

Manuscript received November 25, 2017; accepted for publication June 22, 2018; published online xxxx xx, xxxx.

[1] College of Civil Engineering, Hunan University, Yuelu Mountain, Changsha, Hunan 410082, China, https://orcid.org/0000-0001-8303-1010 (G.Z.)

[2] Department of Civil, Architectural and Environmental Engineering, University of Texas at Austin, 301 E. Dean Keeton, Austin, TX 78712, USA (Corresponding author), e-mail: zornberg@mail.utexas.edu, https://orcid.org/0000-0002-6307-1047

Introduction

Because of its efficient construction and adaptability to varying topographic conditions, the use of soil nailing has expanded into regions previously identified as having

unfavorable soil conditions (Lazarte et al. 2015). This is the case for regions with expansive clays, which are characterized by moisture-induced swelling and shrinkage behavior resulting from cycles of precipitation and evapotranspiration. This special volume change behavior was tested and quantified by a number of in situ and experimental parameters, including swell pressure, potential vertical rise, and other measurable parameters of stress and deformation (Fourie 1989; Brackley and Sanders 1992; Mitchell 1993; Tex-124-E, *Test Procedure for Determining the Potential Vertical Rise*; Thompson, Perko, and Rethamel 2006; Erzin and Erol 2007; Wright, Zornberg, and Aguettant 2007; Hong 2008; Tan 2016).

In certain cases, the construction of foundations, roadways, and retaining walls over expansive clays has been unavoidable. The swell-induced effect on structural response has been evaluated by quantifying the swelling behavior under simplified boundary conditions and modeling the soil's unsaturated suction-moisture relationship (Challa and Poulos 1991; Nelson and Miller 1992; Mohamedzein, Mohamed, and El Sharief 1999; Lytton, Aubeny, and Bulut 2004; Hong 2008; Thomas, Puppala, and Hoyos 2009; Xiao et al. 2011; Sahin 2011; Brown 2013).

For nails embedded in expansive clays, the constrained swelling of the surrounding soil mass upon wetting will cause an increase in the normal stresses acting on the interface, which fundamentally affects the soil-nail interface shear strength. Yet the constrained swell in response to wetting is a function of the initial confining stresses, in which the confining stress corresponding to zero volumetric strains defines the swell pressure (ASTM D4546-14e1, *Standard Test Methods for One-Dimensional Swell and Collapse of Soils*). Due to the impact of soil dilatancy, the swell-induced pressures will vary in the radial direction along with the propagation of interface shear stress. Overall, the nature of the numerous coupled relationships involved in the interaction between nails and the surrounding soil mass is particularly complex for nails embedded in expansive clays. Use of numerical tools to address this complexity has been reported and involve modeling the soil-nail interface behavior via relationships between soil suction and soil hydraulic properties and correlations between volumetric changes and soil confinement (Wu and Pan 2008; Li et al. 2011; Yelti 2011; Bin-Shafique et al. 2013).

In the design of soil nail walls, the ultimate pullout resistance of a soil nail is often estimated by mobilizing the soil-nail interface shear strength over the entire bond area. This assumed uniform distribution of shear stress implies fully developed bond strength and a linear axial force profile over the embedment length. Design guidelines have recommended typical ranges or correlations with field penetration data to estimate the interface bond strength of nails in various soil types (Lazarte et al. 2015). However, pullout tests and direct shear tests remain the most commonly used methods to study the interface shear behavior of soil nailing systems under varied conditions, such as overburden stress, grouting pressure, soil dilation, and the degree of soil saturation (Cheuk, Ng, and Sun 2005; Yin and Su 2006; Su et al. 2007; Zhou and Yin 2008; Yin and Zhou 2009; Su, Yin, and Zhou 2010; Zhou, Yin, and Hong 2011; Hong et al. 2013; Zhou, Yuen, and Tan 2013; Hossain and Yin 2014; Cheng, Au, and Yeung 2016; Wang et al. 2016). It should be noted that the soil-nail interface shear model used in the pullout tests reported was represented by the relationship of average shear stress over the entire bond area against the displacement at the loaded end of the nail and based on the uniform distribution of shear stress as assumed in design codes. However, the profile of axial force along soil nails embedded in expansive clays has been reported as highly nonlinear (Li et al. 2011; Yelti 2011; Bin-Shafique et al. 2013), which is inconsistent with the linear profile that results from assuming a uniform shear stress distribution over the entire soil-nail interface.

It is particularly challenging to obtain the interface shear model of a soil nail in pullout tests when testing a full-length nail. Because it is difficult to ensure the installation of sensors at the appropriate locations within the soil shear band near the interface of interest, the deformation profile of the actual soil surrounding the nail is difficult to determine. An element nail pullout cell was specially designed to address the difficulty involved in capturing key aspects of the various coupled relationships that affect soil-nail interaction, and in determining the shear stress and relative displacement along the interface. Pullout tests were conducted using an embedded soil nail that was 10 cm in length, or only a small fraction of the length of typical nails used in engineering practice. The negligible axial deformation of the element nail and the fully constrained deformation of the surrounding soil mass within the element nail pullout cell made it possible to obtain the magnitude of shear stresses and relative displacements along the interface by identifying the imposed magnitude of the pullout force and pullout displacement, as well as the interface surface area (Chen et al. 2016a, 2016b; Liang et al. 2016).

A specific goal of this study was to characterize the effect of varying moisture conditions on the interface bond strength for nails embedded in expansive clays. An earlier version of the element nail pullout cell was used to characterize the soil-nail interface in nonexpansive, fine-grained soils and evaluate the influence of compaction conditions of the surrounding soils, curing time of the grout, and loading rate of the applied pullout force (Chen et al. 2015). This technique is also suitable for testing soil nails embedded in expansive clays, under varying degrees of saturation, to characterize the appropriate parameters with which to model the shear mechanism of the soil-nail interface.

To validate the applicability of the interface shear model obtained via element nail pullout test results, a large-scale nail pullout test was also conducted as part of this investigation. The large-scale pullout test was carried out after inundation of the expansive clays surrounding the nail to obtain the pullout load–displacement curve. The inundation phase of the test facilitated the measurement of the swell-induced deformation profile of the expansive clays adjacent to the nail inclusion. A theoretical framework was developed to validate the use of element nail pullout test results to predict the results of post-swell large-scale nail pullout tests. The remainder of the article describes the development and implementation of element nail pullout tests to characterize the complicated load transfer process of nails installed in expansive clays.

Material Properties

The soil specimens used throughout the experimental testing program were collected from the Baise Basin, a region in the southwest of the Guangxi Province in China that is characterized by the presence of expansive clays. Soils tested were reconstituted to the target moisture and density conditions. Consistent with JTG E40-2007, *Test Methods of Soils for Highway Engineering* (a Chinese standard), a series of laboratory tests were conducted at Hunan University in China to determine the standard soil properties, as presented in **Table 1**. **Fig. 1** illustrates the relationship between vertical strains (either swell or collapse) and vertical stresses, as obtained by one-dimensional swell/collapse tests conducted in accordance with test method A of ASTM D4546-14e1. The characteristics of the steel bars and cement grout used throughout testing are also listed in **Table 1**.

TABLE 1

Information on materials used throughout testing program.

Property	Information
Clay	
Specific gravity	2.72
Plasticity limit, %	22.93
Liquid limit, %	52.18
Maximum dry density, g/cm^3	1.65
Optimal moisture content, %	18.8
Uniformity coefficient	20.8
Curvature coefficient	0.26
Cement Grout	
Sand type	Medium sand[a]
Cement strength, kPa	42.5
Water ratio, %	45
Grouting method	Gravity
Steel Bar	
Bar type	Hot-rolled ribbed bars
Bar diameter, mm	8
Ultimate tensile stress, MPa	540
Elastic modulus, GPa	231.4
Yield stress, MPa	400

Note: [a] Medium sand is characterized by average diameter ranging from 0.25 to 0.5 mm and fineness modulus ranging from 2.3 to 3.0.

FIG. 1

Volumetric changes as a function of vertical stress for the soil tested in this investigation (tests conducted following test method A of ASTM D4546-14e1).

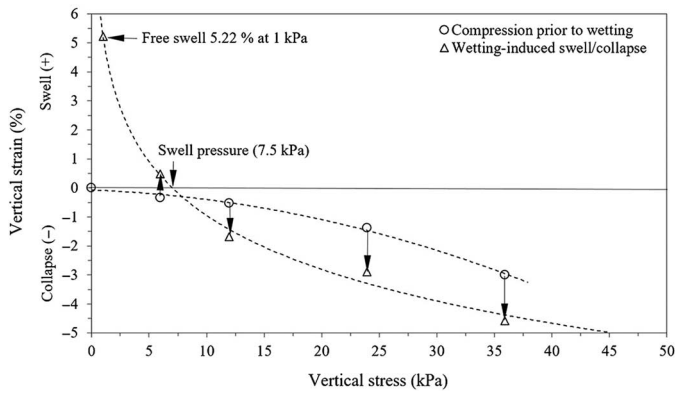

Element Nail Pullout Test

TESTING SCHEME

The element nail pullout testing device was developed by using the Frictional Performance Testing System (FPTS) for the Anchor-Soil Interface available in the geotechnical laboratory of Hunan University (Chen et al. 2015, 2016a, 2016b; Liang et al. 2016) as the basis. A compaction cell was specially designed to hold the soil specimens, as shown in Fig. 2. The specific steps in the testing procedure of this study are as follows:

FIG. 2

Overview of the element nail pullout cell.

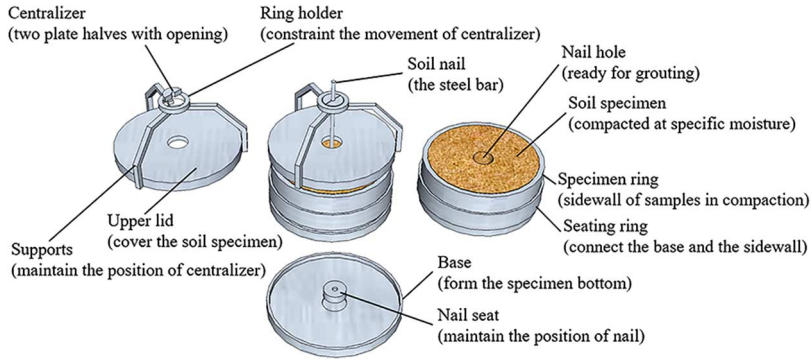

(a) The required quantity of oven-dried expansive soil was sieved through the 5-mm sieve.
(b) The dry soil was moisture-conditioned to the target moisture content and sealed in a plastic bag for over 24 hours, except for the case of saturated specimens, which were prepared by inundation in distilled water for 30 days.
(c) The quantity of soil needed to achieve a target dry density of 1.5 g/cm^3 within the specimen volume was prepared and compacted in five layers (see Fig. 3a).
(d) A preplaced core rod was removed to create a nail hole (see nail hole in Fig. 2).
(e) Cement grout was prepared with a 45 % water ratio, and the nail hole was grouted by gravity with the nail centered therein (see centralizer in Fig. 2).
(f) The grout surrounding the nail was vibrated and densified with an iron stick and continued curing in a sealed plastic bag for 28 days, without the upper lid, to form the nailing (see Fig. 3b).
(g) Excess soils were trimmed to finalize the specimen length at 100 mm. As shown in Fig. 3c, the nail extended 40 mm below the cell base, which allowed for a consistent shearing surface area to be maintained in the pullout process.

A schematic of the completed specimen with cell dimensions is provided in Fig. 4. The effective diameter of the soil-nail interface was 38 mm with a height of 100 mm, resulting in an effective nail specimen with a height/diameter ratio of 2.63. In engineering practice, the diameter of drilled nail holes generally range from 90 to 150 mm, so the corresponding nail length ranges from 237 to 395 mm when considering the height/diameter ratio adopted in this testing setup. In actual soil nailing applications, the typical length of a soil nail is 10 m. Consequently, the setup of the element nail pullout cell effectively

FIG. 3

Steps for specimen preparation in the element nail pullout cell: (a) compaction operations, (b) view of specimen after curing, and (c) specimen view after final trimming.

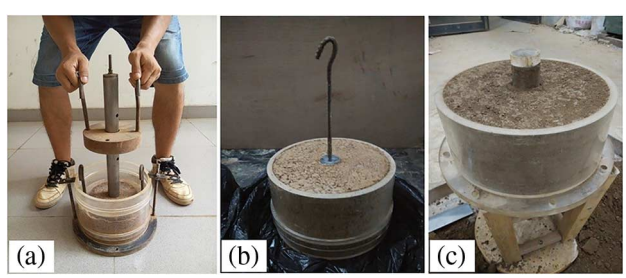

FIG. 4

Schematic of completed specimen in the element nail pullout cell.

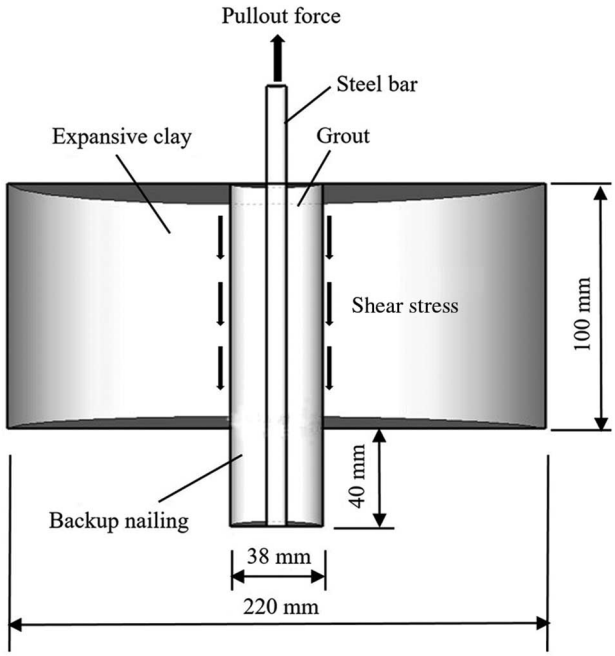

tests the bond strength of a nail segment corresponding to 2.37 to 3.95 % of an actual soil nail. Based on results from research conducted on the settlement analysis of pile foundations (Cooke, Price, and Tarr 1979; Yang and Zai 1994), a ratio of 5.79 between the diameters of the drill hole and the surrounding soils was selected to minimize boundary effects.

Five specimens were prepared at a dry density of 1.5 g/cm^3, with varying degrees of saturation achieved by changing the target moisture content. Each specimen's actual moisture content was measured after dismantling of the pullout tests using samples collected from the soils surrounding the soil-nail interface. **Fig. 5** shows the testing setup, with additional views of the FPTS cell and relevant instrumentation. Pullout loading of all five specimens was carried out by imposing a displacement rate of 1 mm/min. The termination criterion for the nail pullout test was defined as a 20-mm displacement of the nail head, corresponding to a maximum shear strain of 20 % along the interface, which has often been identified as the occurrence of interface shear failure in soil nail pullout tests (Yin and Zhou 2009; Zhou, Yin, and Hong 2011; Cheng, Au, and Yeung 2016).

TEST RESULTS

As presented in **Fig. 6**, shearing failure consistently occurred along the grout-soil interface, indicating that the bar-grout interface provided greater resistance than the grout-soil interface, as expected, particularly for nails installed in expansive clays. Accordingly, and within the context of this study, the soil-nail interface corresponds to the interface defined by the grout and surrounding soil, which corresponds to the weaker of the two interfaces along which failure could occur in a soil-nail system.

The shear stresses along the soil-nail interface were determined by averaging the pullout force across the interface area, which effectively assumes that the stress distribution is uniform. Accordingly, the induced nail movement was also characterized by a constant

FIG. 5

Testing setup of element nail pullout on FPTS.

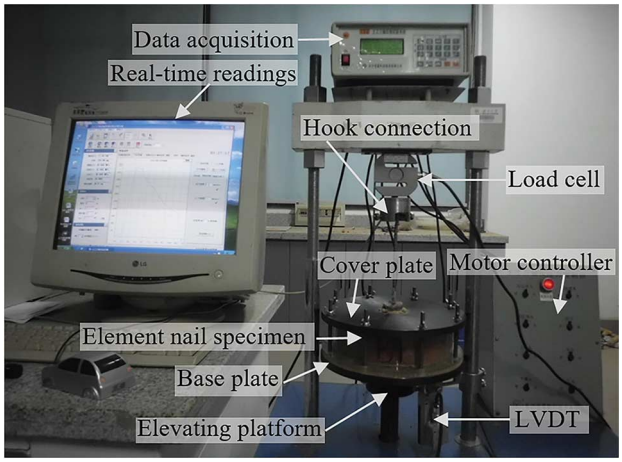

FIG. 6

View of nail-soil interface after pullout failure: (a) view of nail head and (b) view of retrieved nail specimens (moisture content increased from left to right, with leftmost used in trial test).

shear displacement along the entire interface of the element nail. Fig. 7 shows the mobilized shear stresses versus shear displacements imposed on the element nail-soil interface. The shear stress–displacement curves indicate the presence of a postpeak shear strength drop that was found to occur consistently for the various specimens prepared with different degrees of saturation. The shear stress–displacement curves (bond resistance curves) along the interface were found to approximately define three phases, referred to herein as the elastic phase, strain-softening phase, and residual phase. These phases are constrained by two limit points in each profile. The elastic phase involves a reasonably linear increase in shear stress with increasing displacements. The strain-softening phase corresponds to decreasing shear stress after the peak shear strength was reached for continuously increasing displacements. Finally, the residual phase is characterized by plastic flow, in which displacements developed under an essentially constant shear stress. This three-phase trend was found to be more clearly defined in specimens with a comparatively high degree of saturation. However, the softening phase was found to occur for particularly large shear strain values, so the residual phase initiated in some of the curves at strain values greater than the 20 % termination shear strain criterion. In these cases, only

FIG. 7

Shear stress versus shear displacement at various degrees of saturation.

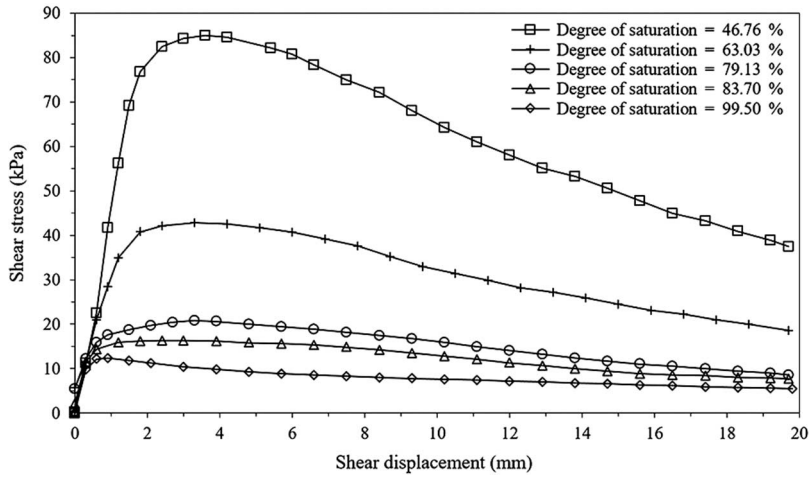

two of the phases could be characterized. The peak shear strength is identified herein as the ultimate bond strength of the soil-nail interface. The results shown in Fig. 8 illustrate that increasing values in the degree of saturation resulted in decreased ultimate bond strengths that can be characterized as exponential. Also, the strength-degrading pattern was fitted using the exponential function, which can be used to predict the ultimate bond strength as a function of the degree of saturation for specimens under the same compaction conditions. For the results in this testing program, the exponential function can be defined as follows:

$$q_u = 671.38e^{-0.0435S_r} \quad (1)$$

where q_u = the ultimate bond strength of the soil-nail interface in expansive clays, kPa; and S_r = the degree of saturation in the expansive clay surrounding the nail, %.

Eq 1 is particularly suitable for predictions involving degree of saturation values ranging from 45 to 100 %, which correspond to the approximate range used in the experimental testing program.

FIG. 8

Ultimate bond strength versus degree of saturation.

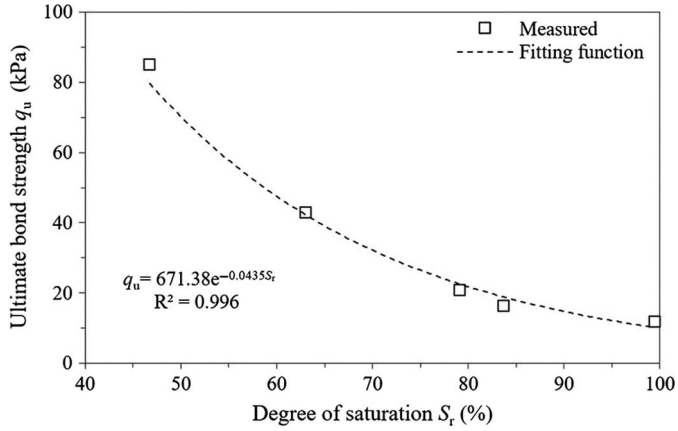

Large-Scale Inundation Test and Post-Swell Pullout Test

Large-scale nail pullout equipment was also developed as part of this study. While the size of the equipment facilitates testing of nails shorter than those typically used in engineering practice, it is considered large scale because it is considerably larger than the element nail pullout cell and provides the information needed to assess the effect of scale in the interpretation of test results. The sample was first subjected to an inundation stage, carried out prior to pullout loading to facilitate decoupling the interaction between swell-induced loading and external loading that would correspond to that of soil nails in service. The moisture-induced swell induced axial displacements that resulted in upward movement of the nail head. Soil displacements were measured at various depths, as well as the movement of the nail head throughout the inundation stage, during which no axial pullout force was externally applied. The pullout force was then applied to the nail after completion of the swelling process of expansive clays, considering that no additional swelling strains would occur and that the development of swell-induced stresses had been stabilized. The magnitude of the pullout force and displacement of the nail head were monitored during the pullout stage of the large-scale test to characterize the resisting mechanisms of a soil nail embedded in expansive clays under post-swell conditions.

TESTING SETUP

A schematic with design information on the large-scale pullout test equipment is presented in Fig. 9. The setup consisted of four main steps, as presented next.

Preparation of the Testing Bin

A steel drum that was 600 mm in diameter and 900 mm in height was used as the testing bin after verification that it met the water tightness requirement of the test's inundation stage. The bottom of the drum was covered by a 100-mm-thick layer of medium dense sand before expansive clays were placed in layers to a maximum height of 600 mm. The clay soils were compacted to a target dry density of 1.5 g/cm^3 by controlling the amount of soil needed to attain the target specimen volume with the target moisture content. The soil placement conditions in the large-scale pullout tests were carefully controlled to achieve the same compaction conditions as those of the specimens tested in the element nail pullout cell. The nail hole was 40 mm in diameter and 600 mm in length, with a 200-mm-high portion of the bin left unfilled to allow for placement of inundating water and space for swelling heave. The diameter of the nail hole was 1/15th of the diameter of the surrounding soils to minimize boundary effects, based on the reported influence zone of interface shear stress in pile settlement analysis (Cooke, Price, and Tarr 1979; Yang and Zai 1994).

Monitoring of Soil Displacements

The swell-induced vertical rise that developed at various embedment depths in the expansive clays is a function of the overburden pressure. Six settlement plates were installed within the expansive clay surrounding the nail at depths ranging from 0 to 500 mm and at a vertical spacing of 100 mm in a circle concentric with the nail holes at a radius of 150 mm using specific circular spacing. Fig. 10 depicts the settlement plate layout, with labels #1 to #6 indicating the relative location of settlement plates and label #7 corresponding to the nail head. Other than settlement plate #1 on the surface, each settlement plate was bolted to a slender lightweight steel thread with a nut head extending above the surface. Each steel thread was

FIG. 9

Schematic of large-scale nail pullout testing setup.

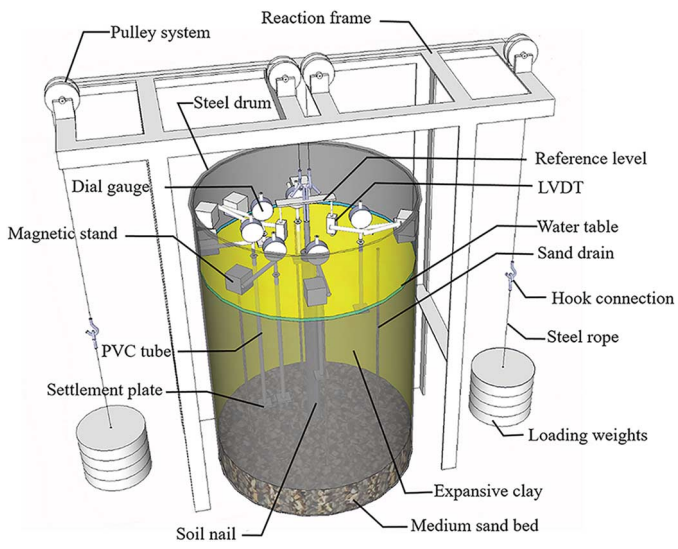

FIG. 10 Setup of instrumentation to measure vertical rise in soil: (a) installation of slender threads, (b) instrumentation layout, and (c) installation of dial gauges.

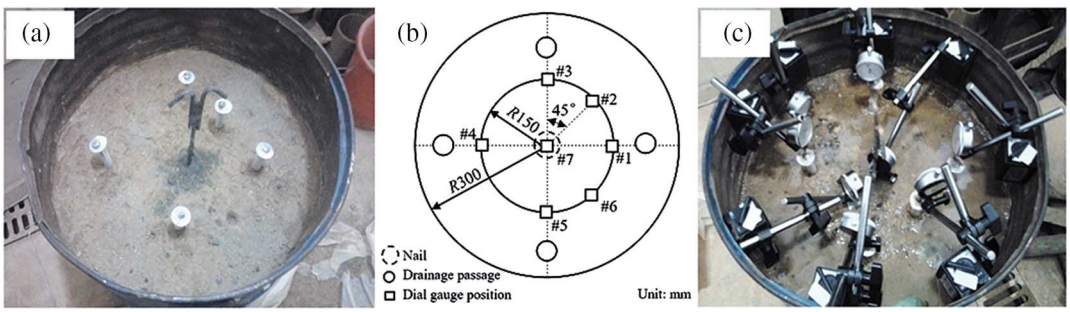

encased in a poly(vinyl chloride) (PVC) tube to facilitate precise measurement of soil displacements at specific positions by isolating the point of measurement from swelling disturbances at other locations (see Fig. 10a). Seven dial gauges were fixed to the steel sidewall of the drum with magnetic stands, which were attached to settlement plate #1, nut heads #2 to #6, and nail head #7, as shown in Fig. 10c. The vertical rise of the soil at each embedment depth was monitored in real time by dial gauge readings. The dial gauge attached to the nail head during the inundation stage was replaced by two linear variable differential transformers (LVDTs) in the pullout loading stage with the tips attached to a reference level.

Accelerated Infiltration

To accelerate infiltration during the inundation stage as well as facilitate a uniform increase in the soil moisture content, four vertical sand drains were installed throughout the expansive clay mass and connected with the sand bed underlying the test bin, forming a horizontal-vertical drainage network. The diameter of the sand drains was 8 mm, and the layout is shown in Fig. 10b.

Loading System

The loading system consisted of a reaction frame, pulley system, steel rope, and loading weights, as illustrated in Fig. 9. Pullout loading was applied by transferring weights suspended by a steel rope with a pulley system. Sand bags were placed under the weights as cushions to prevent collision between the weight and concrete floor upon failure of the soil nail system. The cushion's thickness was selected to ensure that the drop height did not exceed the range of the LVDTs installed to monitor nail head movement.

TESTING STEPS

The inundation and pullout stages of the test were carried out consecutively to facilitate the testing procedure and minimize the influence of creep on the soil sample. The testing steps were as follows:

(a) The clay samples were prepared by sieving particles retained in the 5-mm sieve and moisture-conditioning the soil to a target moisture content of 16.5 %. Samples were sealed in plastic bags for seven days to ensure uniform moisture distribution.
(b) The testing bin was placed on the floor, with a short core rod welded to the bottom center, after which a PVC tube with a 40-mm diameter was attached to the core rod, thus maintaining a free space for the nail hole.
(c) A layer of medium dense sand was placed at the bottom of the drum, forming a sand bed 100 mm thick.
(d) The quantity of expansive clay required to achieve a target dry density of 1.5 g/cm^3 within the cell volume was placed and compacted in six layers. Settlement plates with PVC tube cases were installed at specific locations within the soil mass, and their positions were carefully maintained as the elevations of the different embedded settlement plates could be affected by compaction operations. The exact elevations of the settlement plates were defined using the length of the steel rod connected to settlement plates as reference.
(e) After compaction of the backfill soils was complete, the testing bin was covered in plastic film and moisture was maintained for seven days to facilitate moisture distribution homogenization.
(f) The central PVC tube was extracted and a steel bar with a head hook was inserted into the nail hole using centralizers. The cement grout was injected by gravity and fully densified by vibration. The soil-nail system was covered with plastic film while the grout cured.
(g) Dial gauges affixed by magnetic stands were placed on the nut heads of the slender steel threads, settlement plate, and nail head, as seen in Fig. 10.
(h) After a 28-day curing period, distilled water was poured into the testing bin to achieve a water table elevation that was slightly higher than the ground surface. This corresponded to the beginning of the inundation stage.
(i) Dial gauge readings were recorded every four hours, and the swelling process continued until the rate of vertical rise was under 0.05 mm/day, which was considered as the definition of the completion of the inundation stage.
(j) The dial gauge on the nail head was replaced with two LVDTs installed with their tips attached to a reference level, as shown in Fig. 9, to allow for real-time monitoring of nail head movement.
(k) Pullout load was applied to the nail by attaching hooks to the steel ropes and adding weights to the opposite end from both sides. Since the ultimate pullout resistance was expected to be on the order of 0.5 kN for the tested soil nail (Lazarte et al. 2015), loading steps of 0.05 kN were applied, anticipating a total of ten loading levels. Each loading level was applied when the displacement increment for the current loading

level was below 0.1 mm for over 5 minutes. The pullout stage of the test was terminated when the displacement increment at the current loading level exceeded twice the displacement of the previous loading level.

TESTING RESULTS

Fig. 11 presents two views of the test after pullout failure, one showing the ground surface and the other showing the full soil-nail interface after removal from the testing device. The readings of dial gauges #1 to #6 were used to determine the vertical movements within the expansive soil mass at six different elevations, with the increasing vertical rise shown as a function of time in Fig. 12. While the presence of a soil nail may affect the swelling pattern, the expected increase in vertical strains with decreasing overburden pressures was still observed. The vertical rise of the soil at comparatively deep locations was found to be very small (below 1 mm) during initial stages of the inundation phase, showing a clear increase at a specific time, and remaining essentially constant after such increase. This earlier period in the inundation stage corresponds to the time required for water to permeate to the various elevations within the soil mass. Greater embedment depths corresponded to longer permeating paths and durations of time before the triggering of vertical movements, as can be clearly observed in the curves for depths of 300, 400, and 500 mm.

The time history of the vertical rise at the six locations exhibited trends that can be grouped into four phases. The first is an initiation phase, wherein the swelling rise is

FIG. 11

Pullout failure in large-scale nail pullout test: (a) view of nail head and (b) view of retrieved nail.

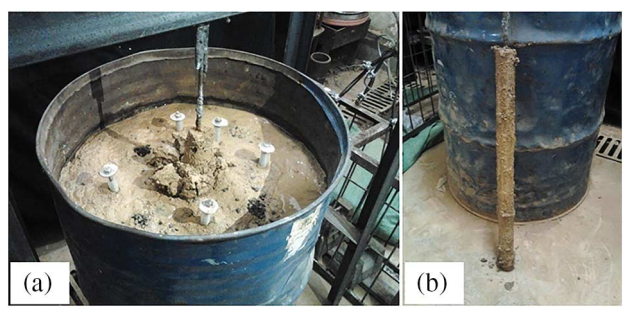

FIG. 12

Vertical rise history of expansive clays at different depths during inundation phase of large-scale test.

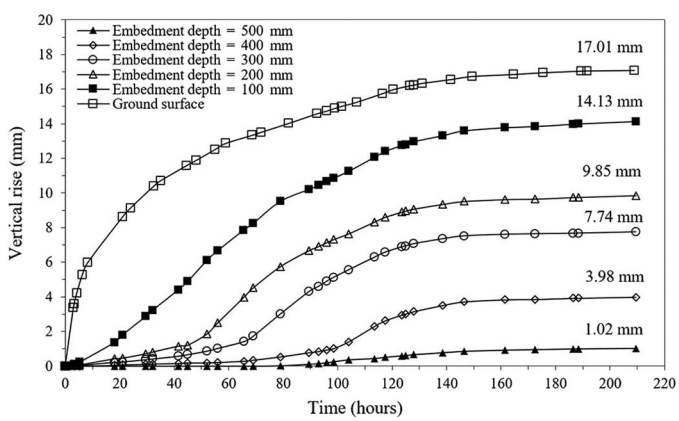

relatively small before water infiltration reaches the corresponding depth. Next is an accelerated rise phase, in which a substantial increase in vertical rise, developing at comparatively high displacement rates, can be observed. The third phase involves a deceleration phase, wherein the rate of vertical displacement decreases, and the fourth phase is the stable phase, in which the swelling rise terminates and results indicate a constant vertical displacement, referred to as the ultimate vertical rise. It should be noted that the change in the rate of vertical rise before reaching the stable phase was not clearly observed for soils at an embedment depth of 100 mm, for which a constant rate of increase was observed rather than a transition from the acceleration phase to the deceleration phase. Fig. 13 shows the ultimate vertical rise versus embedment depth within the soil mass surrounding the nail. As shown in the figure, the relationship between ultimate vertical rise and embedment depth is reasonably linear, which is also consistent with previously reported results (Challa and Poulos 1991; Xiao et al. 2011). Note that there is a certain embedment depth below which no vertical rise could be detected in inundation tests because of the equilibrium between the swell pressure and the overburden pressure, referred to herein as swelling depth limit.

The ultimate swell-induced heave of the nail head obtained from the #7 dial gauge readings was 4.17 mm, while the ultimate vertical rise at the surface, recorded by the #1 dial gauge, was 17.05 mm. Consequently, the relative displacement reached 12.88 mm, as also evidenced by the soil nail head sinking into the expansive clays. Because vertical rise decreases with increasing depth, there should be a specific depth at which the load-induced nail displacement equals the vertical rise of the surrounding soil, that is, where the relative displacement along the soil-nail interface is zero. This specific depth is defined herein as the neutral point, which is consistent with the concept of a neutral point in problems involving negative friction of pile foundations. The movement of the nail relative to the surrounding soil is upward for locations above the neutral point and downward for locations below it. Consequently, the interface shear induced by the soils changes from a lifting to a dragging force at the neutral point. It should also be noted that the relative displacement at the soil-nail interface toward the surface has increased to the value corresponding to the residual phase of the shear stress–shear displacement curves, as shown in Fig. 7.

Although a vertical orientation was found to facilitate practical experimental procedures, it is acknowledged that soil nails in practice are installed into the surrounding soils

FIG. 13

Ultimate vertical rise as a function of embedment depth.

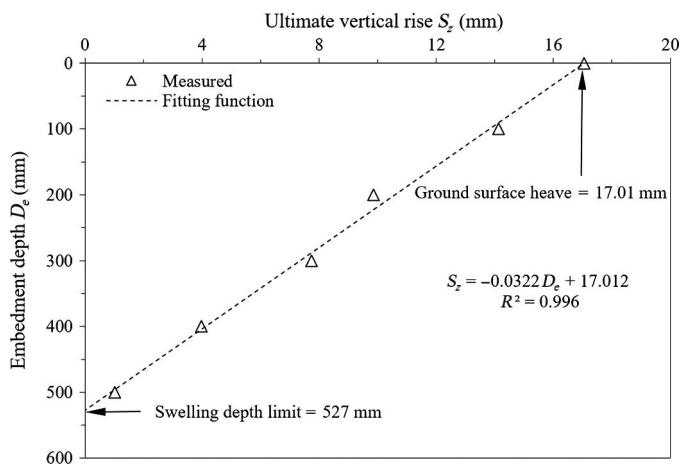

FIG. 14

P-s curve for large-scale nail pullout test.

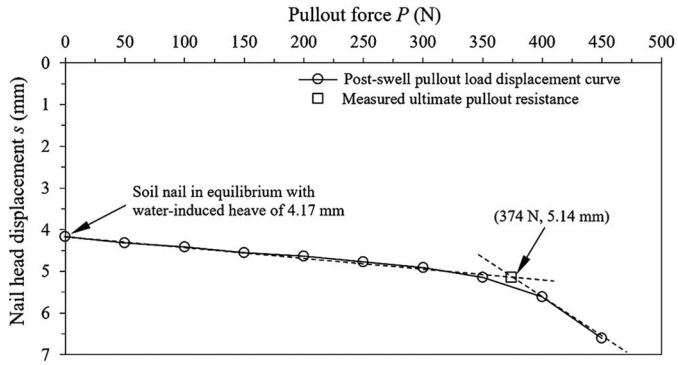

in an approximately horizontal orientation. While additional research is recommended to evaluate the effect of nail orientation on the findings of this investigation, the overall approach is deemed to adequately account for relevant variables, including the soil placement conditions and degree of saturation.

Fig. 14 shows the pullout force as a function of nail head displacement, referred to herein as the *P-s* curve for soil nails, which was obtained during the pullout stage of the large-scale test. Since loading occurred after the inundation phase, nail failure occurred under the combined effects of swelling-induced increased confinement and axial loading. Inspection of the results in Fig. 14 indicates that the measured *P-s* curve shows an approximately bilinear shape, where the increase in displacement rate indicates the onset of nail failure and the initialization of strain softening along the soil-nail interface. The point corresponding to the onset of failure (shown graphically in Fig. 14) was defined in this study as the ultimate pullout resistance of the soil-nail system.

Theoretical Framework for Interpretation of Pullout Test Results

ASSUMPTIONS

The deformation profile within expansive clays during the post-swell pullout process was characterized considering the ultimate vertical rise as measured after the inundation stage of the test. This profile was adopted as the initial condition for the subsequent application of pullout-induced shear stresses. The variation in vertical soil strains in the radial direction induced during the inundation stage are assumed to be negligible. Consequently, the vertical deformations induced during the inundation stage and measured at a radial distance of 150 mm from the nail axis are considered representative of the vertical displacements in the soil mass at that particular depth, including near the soil-nail interface where volumetric strains in the radial direction would have been greatest.

The *r-z* planar coordinate system is adopted herein, where positive directions are considered outward and upward along the radial and axial directions, respectively. The origin of coordinates corresponds to the center of the nail at the base of the system, as depicted in Fig. 15b, which illustrates the analytical model for the large-scale pullout test.

As previously discussed, a swelling depth limit was identified for the vertical rise of expansive clays surrounding a nail, below which swell-induced heave should not be detected. Therefore, the soil mass surrounding the nail was divided into a swelling and nonswelling zone by the depth limit. The magnitude of the depth limit, as measured in the inundation stage of the test, was 527 mm, as identified by the intersection at zero ultimate vertical rise in Fig. 13. This depth limit may exceed the length of the entire nail. Because the analytical framework presented herein was developed to interpret only the large-scale pullout test conducted as part of this study, the swelling and nonswelling zones are only divided along the length of the nail, as seen in Fig. 15. Considering the linear function in Fig. 13, the swell-induced vertical rise can be defined as follows:

$$S(z) = \begin{cases} 0 & 0 \le z \le L - H_0 \\ \frac{1}{S_0} z - \frac{L - H_0}{S_0} & L - H_0 \le z \le L \end{cases} \tag{2}$$

where $S(z)$ = ultimate vertical rise of the expansive soil mass at a given depth z, mm; L = length of the soil nail, mm; S_0 = ultimate vertical rise at the soil surface, mm; and H_0 = swelling depth limit, mm.

The three-phase constitutive relationship characterizing the shear stress versus shear displacement for the soil-nail interface obtained in the element nail pullout test (Fig. 7) can be represented by a trilinear interface shear stress–displacement model, as illustrated in Fig. 16 (Benmokrane, Chennouf, and Mitri 1995; Ren et al. 2010; Ma et al. 2016). The model can be expressed as follows:

$$\tau = k\Delta w + c \tag{3}$$

where the parameters k and c are defined for Phases I, II, and III, respectively, as shown in Fig. 16:

$$\begin{cases} k = k_1 = \frac{\tau_1}{w_1} & c = c_1 = 0 & \text{for } 0 \le \Delta w \le w_1 \\ k = k_2 = \frac{\tau_2 - \tau_1}{w_2 - w_1} & c = c_2 = \frac{\tau_1 w_2 - \tau_2 w_1}{w_2 - w_1} & \text{for } w_1 \le \Delta w \le w_2 \\ k = k_3 = 0 & c = c_3 = \tau_2 & \text{for } \Delta w \ge w_2 \end{cases} \tag{4}$$

FIG. 15

Schematic of load transfer model for interpretation of large-scale post-swell pullout test: (a) control element, (b) overview of soil nail and numerical discretization, and (c) shear displacement distribution.

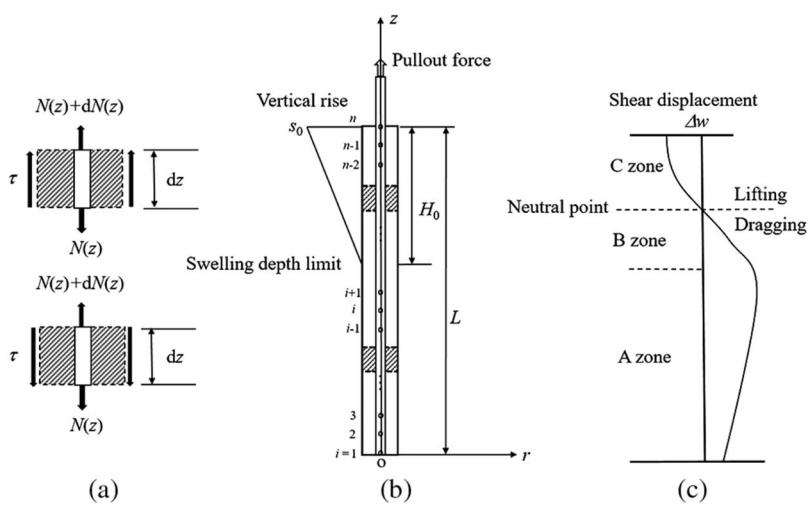

FIG. 16

Schematic of trilinear interface shear stress–displacement model.

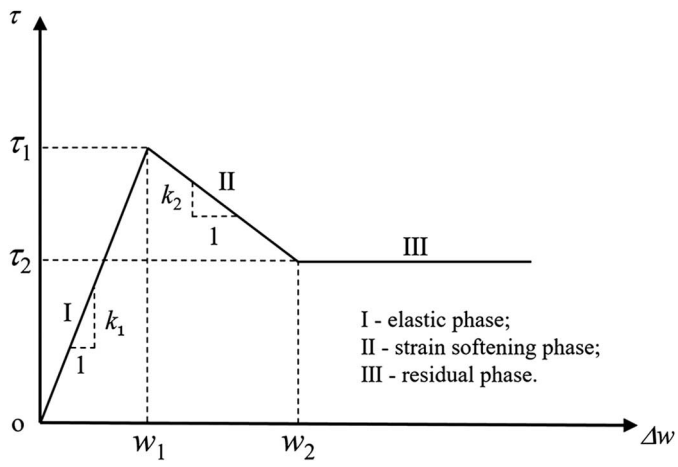

where τ = shear stress along the soil-nail interface, kPa; Δw = shear displacement (relative displacement) along the soil-nail interface, mm; τ_1 = peak shear strength (i.e., ultimate bond strength), kPa; τ_2 = residual shear strength, kPa; w_1 = shear displacement at peak shear strength, mm; and w_2 = shear displacement corresponding to the onset of residual shear strength, mm.

It should be noted that values for the parameters in the interface shear stress–displacement model depend on the degree of saturation of the expansive clays surrounding the nail, as observed in the set of results shown in Fig. 7. The trilinear model reduces to a bilinear model when the value of w_2 is significantly large, which indicates a softening phase so long that the residual phase is not reached. This was the case for the results of tests conducted at a comparatively high degree of saturation.

A linear variation of moisture content versus embedment depth in the swelling zone and a constant moisture condition in the nonswelling zone were adopted in accordance with this observation (Challa and Poulos 1991). This assumption implies that during the inundation stage the water front did not progress beyond a depth at which no swell-induced rise was observed. However, in reality, the magnitude of swelling strains are a function of overburden pressure, as shown in Fig. 1, so the depth at which no deformation was detected probably experienced wetting but under overburden pressures that exceeded the swell pressure. The mean value of the degree of saturation in the swelling zone was found to be 76.9 %, while the initial degree of saturation observed in the nonswelling zone was 55.2 %. These values for degrees of saturation were adopted for interpolation of the results presented in Fig. 7 to define the relevant parameters for the trilinear model, as shown in Table 2.

LOAD TRANSFER MODEL

Similarity between the resisting mechanisms of soil nails and pile foundations in expansive clays (Challa and Poulos 1991; Wang et al. 2008; Brown 2013) prompted incorporation of concepts used in the analysis of negative friction in axially loaded single piles into this study's load transfer analysis of soil nails in expansive clays observed in pullout testing.

TABLE 2
Calculation parameters in load transfer model for theoretical interpretation.

Parameters	Value	Data Sources
$[S_0, H_0]$ in Eq 2	[17.05 mm, 527 mm]	Intercept of linear function in Fig. 13
$[L, D, E]$ in Eqs 5–14	[600 mm, 40 mm, 20 GPa]	Setup of large-scale pullout test
$[w_1, \tau_1, w_2, \tau_2]$ in Eq 4	[4.5 mm, 85.58 kPa, 20.0 mm, 37.5 kPa]	Interpolation using Fig. 7 and Eq 1 for initial degree of saturation of soil over nail length $(L - H_0)$
	[3.0 mm, 25.07 kPa, 8.0 mm, 13.01 kPa]	Interpolation using Fig. 7 and Eq 1 for average degree of saturation of soil over nail length H_0

In the inundation stage of testing, the swelling of expansive clays manifested itself as: (1) a measured vertical rise of the surrounding soils; (2) an additional normal stress acting radially on the soil-nail interface; and (3) shear stresses along the soil-nail interface that resulted in a lifting/dragging tendency of the nail, even in the absence of external loads. In the upper zone of the testing setup, labeled as the C zone in Fig. 15c, the soils surrounding the nail displaced upward in relation to the nail, generating an upward shear that tended to lift the nail. On the other hand, in the lower zone of the testing setup below the neutral point, the nail was the component that displaced upward in relation to the surrounding soil, resulting in dragging forces. These zones are shown as the B zone (within the swelling zone) and the A zone (within the nonswelling zone) in Fig. 15.

In the load transfer analysis, the loads applied to the nail involve initial lifting forces in the form of shear stresses applied during swelling, followed by pullout forces in the form of an external tension, as illustrated in Fig. 15. The initial displacement field along the nail facilitates determination of the shear displacement along the soil-nail interface. Accordingly, the relative displacement between the nail and surrounding soils can be obtained via the pattern of vertical rise with depth, as defined by Eq 2. The shear displacement values can now be used to determine the corresponding shear stresses along the soil-nail interface by means of the trilinear shear model expressed in Eqs 3 and 4. The final determination of the displacement field along the nail involves implementing a t-z analysis for settlement prediction to be conducted following an approach similar to those developed for vertical pile foundations (Poulos and Davis 1980).

The force analysis illustrated in Fig. 15a corresponds to that of a control element of the nail. The force equilibrium and axial stress-strain relationship are as follows:

$$N(z) = \frac{\pi D^2 E}{4} \frac{\partial w(z)}{\partial z} \tag{5}$$

$$\frac{\partial N(z)}{\partial z} = \mp \pi D \tau(z) \tag{6}$$

where $N(z)$ = axial force of the nail at a given depth z, N; $w(z)$ = vertical displacement of the nail at a given depth z, mm; $\tau(z)$ = shear stress distribution along the soil-nail interface at a given depth z, kPa; D = diameter of the nail, mm; and E = elastic modulus of the nail, GPa.

Combining Eqs 5 and 6 results in a differential equation governing the equilibrium of the nail element as follows:

$$\frac{\partial^2 w(z)}{\partial z^2} = \mp \frac{4}{DE}\tau(z) \tag{7}$$

The absolute value of shear displacement along the soil-nail interface can be obtained as follows:

$$\Delta w = |S(z) - w(z)| \tag{8}$$

Substitution of Eqs 3 and 8 into Eq 7 results in the following:

$$\frac{\partial^2 w(z)}{\partial z^2} = \mp \frac{4}{DE}(k|S(z) - w(z)| + c) \tag{9}$$

It should be noted that the negative shear stress in Eqs 6–9 corresponds to the dragging forces in the B and A zones, where the magnitude of the nail vertical displacement $w(z)$ is greater than the vertical rise of the soil $S(z)$, as shown in the lower portion of Fig. 15a. For the control element in the C zone that is depicted in the upper portion of Fig. 15a, the shear stress is positive, representing the lifting force above the neutral point.

NUMERICAL IMPLEMENTATION OF THE LOAD TRANSFER MODEL

A numerical tool based on the finite difference method (Hyett, Moosavi, and Bawden 1996; Ma et al. 2016) was adopted to solve the load transfer model in Eq 9. To implement this approach, the nail was discretized into $n-1$ segments with the same length ΔL (defined as $L/(n-1)$) using n nodes numbered 1 through n starting from the bottom of the nail, as shown in Fig. 15b. In the r-z planar coordinate system seen in Fig. 15b, the vertical coordinates of all nodes can be denoted by $z_i = (i-1)L/(n-1)$.

Thus, the governing differential equation can be rewritten as follows:

for $S(z) > w(z)$,

$$\frac{\frac{w(z_{i+1})-w(z_i)}{z_{i+1}-z_i} - \frac{w(z_i)-w(z_{i-1})}{z_i-z_{i-1}}}{\frac{z_{i+1}-z_{i-1}}{2}} + \frac{4k(z_i)}{DE}w(z_i) - \frac{4k(z_i)}{DE}S(z_i) = \frac{4}{DE}c(z_i) \tag{10}$$

for $S(z) \le w(z)$,

$$\frac{\frac{w(z_{i+1})-w(z_i)}{z_{i+1}-z_i} - \frac{w(z_i)-w(z_{i-1})}{z_i-z_{i-1}}}{\frac{z_{i+1}-z_{i-1}}{2}} + \frac{4k(z_i)}{DE}w(z_i) - \frac{4k(z_i)}{DE}S(z_i) = -\frac{4}{DE}c(z_i) \tag{11}$$

where $k(z_i)$ and $c(z_i)$ can be determined by using $S(z_i)$ from Eq 2 and substituting $w(z_i)$ into Eqs 8 and 4.

Eqs 10 and 11 can be rearranged in terms of nail nodal displacements as follows:

$$\begin{aligned}&\frac{DE}{4(z_i - z_{i-1})}w(z_{i-1}) + \left[k(z_i)\frac{z_{i+1} - z_{i-1}}{2} - \frac{DE}{4(z_{i+1} - z_i)} - \frac{DE}{4(z_i - z_{i-1})}\right]w(z_i)\\ &+ \frac{DE}{4(z_{i+1} - z_i)}w(z_{i+1}) = k(z_i)\frac{z_{i+1} - z_{i-1}}{2}S(z_i) \pm \frac{z_{i+1} - z_{i-1}}{2}c(z_i)\end{aligned} \tag{12}$$

The boundary conditions at the free end and loaded end, i.e., node $i = 1$ and $i = n$, respectively, can be expressed as follows:

$$\left[k(z_1)\frac{z_2-z_1}{2}-\frac{DE}{4(z_2-z_1)}\right]w(z_1)+\frac{DE}{4(z_2-z_1)}w(z_2)=k(z_1)\frac{z_2-z_1}{2}S(z_1)-\frac{z_2-z_1}{2}c(z_1) \tag{13}$$

$$\begin{aligned}&\frac{DE}{4(z_n-z_{n-1})}w(z_{n-1})+\left[k(z_n)\frac{z_n-z_{n-1}}{2}-\frac{DE}{4(z_n-z_{n-1})}\right]w(z_n)+\\ &P_{\text{pre}}=k(z_n)\frac{z_n-z_{n-1}}{2}S(z_n)\pm\frac{z_n-z_{n-1}}{2}c(z_n)\end{aligned} \tag{14}$$

where P_{pre} = the prediction of pullout force applied at the nail head, N.

The iterative steps followed to obtain the solution of nodal displacements for the nail are as follows:

(a) The nodal displacement at the bottom of the nail $w(z_1)$ is specified for a given pullout force P_{loaded}.
(b) The interface shear displacement at this nail node $\Delta w(z_1)$, is obtained by placing $w(z_1)$ and $S(z_1)$ (from Eq 2) into Eq 8. Using $\Delta w(z_1)$ in Eq 4 yields the magnitudes of $k(z_1)$ and $c(z_1)$.
(c) The values of $w(z_1), k(z_1)$, and $c(z_1)$, obtained in Step b, are then used in Eq 13, leading to a new value $w(z_2)$, obtained by repeating Step b on the node with coordinate z_2 to solve $k(z_2)$ and $c(z_2)$.
(d) The calculations in Steps b and c are repeated to determine the remaining values of $w(z_i)$ through Eq 12, with the magnitude of P_{pre} being determined using Eq 14.
(e) The termination criterion for the iterative process was adopted as $|(P_{\text{pre}}/P_{\text{loaded}})-1| < 0.01$. Accordingly, the nodal displacement results were considered as the final output if this criterion was satisfied. Otherwise, the value of $w(z_1)$ should be updated by an increment, and the calculation steps repeated until the termination criterion is satisfied.
(f) The calculated nodal displacements of the nail were used to determine the shear displacement profile related to Eqs 2 and 8, the shear stress distribution using Eqs 3 and 4, and the axial force profile using Eq 5, along the entire length of the nail.

COMPARISON BETWEEN PREDICTED AND MEASURED LARGE-SCALE PULLOUT TEST RESULTS

The head displacement versus pullout force in the large-scale pullout test were predicted using the theoretical framework for load transfer, with input values from a series of tests conducted using the element nail pullout cell. The values for the different parameters used in the prediction, along with the corresponding sources, are provided in **Table 2**. Note that the moisture content of the soils surrounding the nail, measured after completion of the large-scale pullout test, exhibited a similar variation along the length of the nail as that previously assumed (Challa and Poulos 1991).

The predicted values for the pullout force and nail head displacement, as obtained via the theoretical framework and aforementioned iterative procedure, are presented in **Fig. 17**. The figure also compares the predicted values with the measured results obtained from the large-scale post-swell pullout test. It should be noted that the bilinear fitting was used to approximately characterize the pullout force–displacement profile, in which the slope change indicates the transition of the interface shear stress from the elastic phase to the elastic-softening phase, as shown in **Fig. 16**. The elastic limit corresponding to the transition, as determined in **Fig. 17**, was adopted to define the ultimate pullout resistance

FIG. 17

Comparison of measured and predicted *P-s* curve for large-scale nail pullout test in expansive clays.

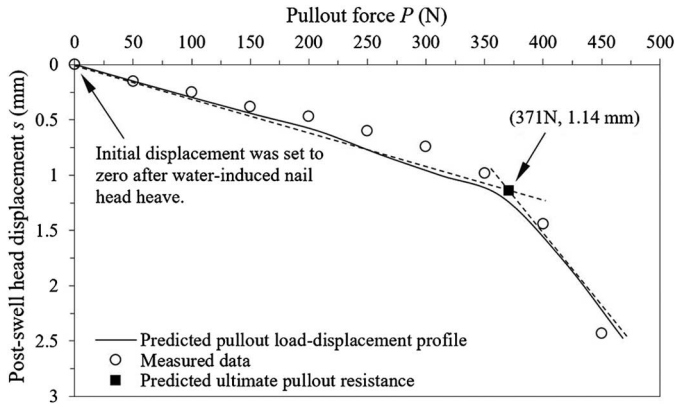

TABLE 3

Comparison of measured and predicted pullout results.

Ultimate Post-Swell Nail Head Displacement, mm			Ultimate Pullout Resistance, N		
Measurement	Prediction	Relative Difference, %	Measurement	Prediction	Relative Difference, %
0.97	1.14	17.5	374	371	0.8

of the nail, which corresponds to the onset of interface shear softening along the entire length of the nail. In addition, the nail head displacements were zeroed at the end of the inundation phase, so the displacements shown in the figure correspond to those induced by pullout loading.

As Fig. 17 illustrates, the measured data show very good agreement with the predicted pullout load–displacement results for the entire range of the test. In particular, the predicted ultimate pullout resistance and post-swell head displacement were found to correspond well with the experimental values obtained from the large-scale pullout test, as documented in Table 3. The predicted ultimate pullout resistance was determined to be within 0.8 % of the value measured experimentally. On the other hand, the predicted ultimate post-swell nail head displacement was determined to be 17.5 % smaller than the measured displacement (see also Figs. 14 and 17).

The suitability of the element nail pullout device for testing soil nails in expansive clays was demonstrated in this study and provides an alternative experimental approach that avoids some of the significant problems encountered in full-length soil nail tests, particularly when involving expansive clays.

Conclusions

An element nail pullout cell was developed to characterize the soil-nail interface of nails installed in expansive clays under controlled moisture conditions. Inundation and post-swell pullout tests were also conducted using a large-scale experimental setup, which allowed for separate evaluation of the swell-induced and pullout-induced responses. A theoretical framework to evaluate nail pullout data generated at different scales was developed as well. In particular, the results from the large-scale pullout test were compared

with predictions obtained via the theoretical framework and results from element nail pullout tests. The following conclusions can be drawn from this investigation:

- The newly developed element nail pullout cell was determined to allow control of key factors that govern the soil-nail interface response, including placement conditions and degree of saturation of expansive clays.
- The response of the nail–grout–expansive soil system was found to be governed by the grout–expansive soil interface, which exhibited a response that could be characterized by a trilinear relationship between shear stresses and shear displacements (for expansive clays with a comparatively high degree of saturation) or by a bilinear relationship (for expansive clays with a comparatively low degree of saturation).
- The ultimate bond strength of the soil-nail interface was found to decrease exponentially with increasing degrees of saturation of the surrounding expansive clays.
- The setup adopted for large-scale nail pullout tests facilitated characterization of the effect of soil swelling on nail inclusions, as the surrounding expansive clays not only rose, but the nail also exhibited lifting movements. The profile of ultimate vertical rise versus embedment depth was found to exhibit a linearly decreasing trend from the soil surface.
- A simplified load transfer analytical framework was developed to capitalize on the generation of experimental results from element nail pullout tests.
- The pullout load versus nail head displacement curve predicted using the analytical framework and input data from element nail pullout tests was found to compare very well with the experimentally measured curve obtained from the large-scale nail pullout test.
- In particular, the predicted nail pullout resistance and post-swell nail head displacement were found to correspond well with the experimental results from the large-scale pullout test.

Overall, this study provides insight into new experimental techniques for the characterization of soil nails installed in expansive clays, which are subjected to particularly complex, coupled interactions between swelling and pullout load transfer mechanisms. However, it should be noted that a soil nail embedded in expansive soils in practice is typically under conditions of drying-wetting cycles, which leads to a complex effect of swelling on the pullout response.

ACKNOWLEDGMENTS

This research was sponsored by the National Natural Science Foundation of China (Contract No. 50878082) and the China Scholarship Council (Contract No. 201506130020). The authors appreciate their support. The insightful comments of the reviewers, which enhanced the content of this article, are also gratefully acknowledged by the authors.

References

ASTM D4546-14, 2014, *Standard Test Methods for One-Dimensional Swell or Collapse of Soils*, ASTM International, West Conshohocken, PA, www.astm.org

Benmokrane, B., Chennouf, A., and Mitri, H. S., 1995, "Laboratory Evaluation of Cement-Based Grouts and Grouted Rock Anchors," *Int. J. Rock Mech. Min. Sci.*, Vol. 32, No. 7, pp. 633–642, https://doi.org/10.1016/0148-9062(96)85147-3

Bin-Shafique, S., Sadat, M., Rahman, S., and Huang, J., 2013, "Performance of Soil Nail Wall in High Plasticity Expansive Soil," presented at the *Geo-Congress 2013, Stability and Performance of Slopes and Embankments III*, San Diego, CA,

Geo-Institute of American Society of Civil Engineers, Reston, VA, https://doi.org/10.1061/9780784412787.178

Brackley, I. J. A. and Sanders, P. J., 1992, "In Situ Measurement of Total Natural Horizontal Stresses in an Expansive Clay," *Géotechnique*, Vol. 42, No. 3, pp. 443–451, https://doi.org/10.1680/geot.1992.42.3.443

Brown, A. C., 2013, "The Behavior of Drilled Shaft Retaining Walls in Expansive Clay Soils," Ph.D. thesis, The University of Texas, Austin, TX.

Challa, P. K. and Poulos, H. G., 1991, "Behavior of Single Pile in Expansive Clay," *Geotech. Eng.*, Vol. 22, No. 2, pp. 189–216.

Chen, C.-F., Liang, G.-T., Liu, X.-M., Tang, Y., Xu, Y.-L., Liu, J.-B., Zhao, Y., and Li, R.-F., 2016a, A device and method for preparing soil samples used in testing frictional performance of anchor/pile-soil interface, China Patent ZL 2014 1 0176979.8, filed April 29, 2014, and issued July 6, 2016.

Chen, C.-F., Liang, G.-T., Tang, Y., and Xu, Y.-L., 2015, "Anchoring Solid-Soil Interface Behavior Using a Novel Laboratory Testing Technique," *Chin. J. Geotech. Eng.*, Vol. 37, No. 6, pp. 1115–1122, https://doi.org/10.11779/cjge201506018

Chen, C.-F., Liang, G.-T., Zhang, G.-B., Tang, Y., Zheng, X.-X., Sun, Y., Wang, S.-Y., and Wang, C.-Z., 2016b, A testing system and method for frictional performance of anchor/pile-soil interface, China Patent ZL 2014 1 0176877.6, filed April 29, 2014, and issued March 30, 2016.

Cheng, Y. M., Au, S. K., and Yeung, A. T., 2016, "Laboratory and Field Evaluation of Several Types of Soil Nails for Different Geological Conditions," *Can. Geotech. J.*, Vol. 53, No. 4, pp. 634–645, https://doi.org/10.1139/cgj-2015-0267

Cheuk, C. Y., Ng, C. W. W., and Sun, H. W., 2005, "Numerical Experiments of Soil Nails in Loose Fill Slopes Subjected to Rainfall Infiltration Effects," *Comput. Geotech.*, Vol. 32, No. 4, pp. 290–303, https://doi.org/10.1016/j.compgeo.2005.02.005

Cooke, R. W., Price, G., and Tarr, K., 1979, "Jacked Piles in London Clay: A Study of Load Transfer and Settlement under Working Conditions," *Géotechnique*, Vol. 29, No. 2, pp. 113–147, https://doi.org/10.1680/geot.1979.29.2.113

Erzin, Y. and Erol, O., 2007, "Swell Pressure Prediction by Suction Methods," *Eng. Geol.*, Vol. 92, Nos. 3-4, pp. 133–145, https://doi.org/10.1016/j.enggeo.2007.04.002

Fourie, A. B., 1989, "Laboratory Evaluation of Lateral Swelling Pressure," *J. Geotech. Eng.*, Vol. 115, No. 10, pp. 1481–1486, https://doi.org/10.1061/(asce)0733-9410(1989)115:10(1481)

Hong, C.-Y., Yin, J.-H., Pei, H.-F., and Zhou, W.-H., 2013, "Experimental Study on the Pullout Resistance of Pressure-Grouted Soil Nails in the Field," *Can. Geotech. J.*, Vol. 50, No. 7, pp. 693–704, https://doi.org/10.1139/cgj-2012-0103

Hong, G. T., 2008, "Earth Pressures and Deformations in Civil Infrastructure in Expansive Soils," Ph.D. thesis, Texas A&M University, College Station, TX.

Hossain, A. and Yin, J.-H., 2014, "Behavior of a Pressure-Grouted Soil-Cement Interface in Direct Shear Test," *Int. J. Geomech.*, Vol. 14, No. 1, pp. 101–109, https://doi.org/10.1061/(ASCE)GM.1943-5622.0000301

Hyett, A. J., Moosavi, M., and Bawden, W. F., 1996, "Load Distribution along Fully Grouted Bolts, with Emphasis on Cable Bolt Reinforcement," *Int. J. Numer. Anal. Methods Geomech.*, Vol. 20, No. 7, pp. 517–544, https://doi.org/10.1002/(SICI)1096-9853(199607)20:7<517::AID-NAG833>3.0.CO;2-L

JTG E40-2007, *Test Methods of Soils for Highway Engineering*, Ministry of Transportation of China, Beijing, China, www.codeofchina.com

Lazarte, C. A., Robinson, H., Gomez, J. E., Baxter, A., Cadden, A., and Berg, R., 2015, "Geotechnical Engineering Circular No. 7, Soil Nail Walls-Reference Manual," Report No. FHWA-NHI-14-007, Federal Highway Administration, Washington, D.C.

Li, J.-H., Zhu, F.-C., Zuo, M.-H., and Yang, Y., 2011, "Finite Element Analysis of Soil Nailing in Expansive Soils Considering Rainfall Effects," presented at the *GeoHunan International Conference 2011*, Hunan, China, American Society of Civil Engineers, Reston, VA, https://doi.org/10.1061/47630(409)12

Liang, G.-T., Chen, C.-F., Luo, H., Xu, Y.-L., Zhang, G.-B., Zhao, H.-B., Mi, W., and Zhao, X.-L., 2016, A device and method for preparing specimens used in testing frictional performance of anchor/pile-soil interface, China Patent ZL 2014 1 0176977.9, filed April 29, 2014, and issued September 28, 2016.

Lytton, R., Aubeny, C., and Bulut, R., 2004, *Design Procedure for Pavements on Expansive Soils: Volume 1, Report No. FHWA/TX-05/0-4518-1*, Texas A&M University, College Station, TX, 198p.

Ma, S., Zhao, Z., Nie, W., and Gui, Y., 2016, "A Numerical Model of Fully Grouted Bolts Considering the Tri-linear Shear Bond-Slip Model," *Tunnelling Underground Space Technol.*, Vol. 54, pp. 73–80, https://doi.org/10.1016/j.tust.2016.01.033

Mitchell, J. K., 1993, *Fundamentals of Soil Behavior*, 2nd ed., John Wiley & Sons, Hoboken, NJ, 437p.

Mohamedzein, Y. E.-A., Mohamed, M. G., and El Sharief, A. M., 1999, "Finite Element Analysis of Short Piles in Expansive Soils," *Comput. Geotech.*, Vol. 24, No. 3, pp. 231–243, https://doi.org/10.1016/S0266-352X(99)00008-7

Nelson, J. D. and Miller, D. J., 1992, *Expansive Soils: Problems and Practice in Foundation and Pavement Engineering*, John Wiley & Sons, Hoboken, NJ, 259p.

Poulos, H. G. and Davis, E. H., 1980, *Pile Foundation and Design (Wiley Series in Geotechnical Engineering)*, 1st ed., John Wiley & Sons, Hoboken, NJ, 397p.

Ren, F. F., Yang, Z. J., Chen, J. F., and Chen, W. W., 2010, "An Analytical Analysis of the Full-Range Behavior of Grouted Rockbolts Based on a Tri-linear Bond-Slip Model," *Constr. Build. Mater.*, Vol. 24, No. 3, pp. 361–370, https://doi.org/10.1016/j.conbuildmat.2009.08.021

Sahin, H., 2011, "Characterization of Expansive Soil for Retaining Wall Design," M.S. thesis, Texas A&M University, College Station, TX.

Su, L.-J., Chan, T. C. F., Shiu, Y. K., Cheung, T., and Yin, J.-H., 2007, "Influence of Degree of Saturation on Soil Nail Pull-Out Resistance in Compacted Completely Decomposed Granite Fill," *Can. Geotech. J.*, Vol. 44, No. 11, pp. 1314–1328, https://doi.org/10.1139/T07-056

Su, L.-J., Yin, J.-H., and Zhou, W.-H., 2010, "Influence of Overburden Pressure and Soil Dilation on Soil Nail Pull-Out Resistance," *Comput. Geotech.*, Vol. 37, No. 4, pp. 555–564, https://doi.org/10.1016/j.compgeo.2010.03.004

Tan, Y., 2016, "Swelling Pressure and Retaining Wall Design in Expansive Soils," M.S. thesis, RMIT University, Melbourne, Australia.

Tex-124-E, 1999, *Test Procedure for Determining the Potential Vertical Rise*, Texas Department of Transportation, Austin, TX, www.txdot.gov

Thomas, M. G., Puppala, A. J., and Hoyos, L. R., 2009, "Influence of Swell Pressure from Expansive Fill on Retaining Wall Stability," presented at the *International Foundation Congress and Equipment Expo*, Orlando, FL, American Society of Civil Engineers, Reston, VA, https://doi.org/10.1061/41023(337)75

Thompson, R. W., Perko, H. A., and Rethamel, W. D., 2006, "Comparison of Constant Volume Swell Pressure and Oedometer Load-Back Pressure," presented at the *Fourth International Conference on Unsaturated Soils*, Carefree, AZ, American Society of Civil Engineers, Reston, VA, https://doi.org/10.1061/40802(189)150

Wang, H., Cheng, J.-H., Guo, Y.-C., and Gao, X.-Y., 2016, "Failure Mechanism of Soil Nail-Prestressed Anchor Composite Retaining Structure," *Geotech. Geol. Eng.*, Vol. 34, No. 6, pp. 1889–1898, https://doi.org/10.1007/s10706-016-9998-5

Wang, N.-X., Gu, R.-W., Zhang, W.-M., and Gu, X.-W., 2008, "Model Tests on Behavior of Single Pile in Expansive Soil," *Chin. J. Geotech. Eng.*, Vol. 30, No. 1, pp. 56–60.

Wright, S. G., Zornberg, J. G., and Aguettant, J. E., 2007, *The Fully Softened Shear Strength of High Plasticity Clays, Report No. FHWA/TX-07/0-5202-3*, The University of Texas, Austin, TX, 132p.

Wu, S.-C. and Pan, D.-G., 2008, "Reinforcement Approach of Self-Balance Pre-stressed Bolts for Expansive Soil Slope," *Chin. J. Geotech. Eng.*, Vol. 30, No. 4, pp. 492–497.

Xiao, H.-B., Zhang, C.-S., Wang, Y.-H., and Fan, Z.-H., 2011, "Pile-Soil Interaction in Expansive Soil Foundation: Analytical Solution and Numerical Simulation," *Int. J.*

Geomech., Vol. 11, No. 3, pp. 159–166, https://doi.org/10.1061/(ASCE)GM.1943-5622.0000046

Yang, R. and Zai, J., 1994, "The Principle of the Generalized Shear Displacement Method for Analyzing the Nonlinear Interaction of Pile-Soil-Pile Cap," *Chin. J. Geotech. Eng.*, Vol. 16, No. 6, pp. 103–116.

Yelti, N., 2011, "Analysis and Design of Soil Nail Walls in High Plasticity Clays," M.S. thesis, The University of Texas, San Antonio, TX.

Yin, J. H. and Su, L.-J., 2006, "An Innovative Laboratory Box for Testing Nail Pull-Out Resistance in Soil," *Geotech. Test. J.*, Vol. 29, No. 6, pp. 451–461, https://doi.org/10.1520/GTJ100216

Yin, J.-H. and Zhou, W.-H., 2009, "Influence of Grouting Pressure and Overburden Stress on the Interface Resistance of a Soil Nail," *J. Geotech. Geoenviron. Eng.*, Vol. 135, No. 9, pp. 1198–1208, https://doi.org/10.1061/(ASCE)GT.1943-5606.0000045

Zhou, W.-H. and Yin, J.-H., 2008, "A Simple Mathematical Model for Soil Nail and Soil Interaction Analysis," *Comput. Geotech.*, Vol. 35, No. 3, pp. 479–488, https://doi.org/10.1016/j.compgeo.2007.07.001

Zhou, W.-H., Yin, J.-H., and Hong, C.-Y., 2011, "Finite Element Modelling of Pullout Testing on a Soil Nail in a Pullout Box under Different Overburden and Grouting Pressures," *Can. Geotech. J.*, Vol. 48, No. 4, pp. 557–567, https://doi.org/10.1139/T10-086

Zhou, W.-H., Yuen, K.-V., and Tan, F., 2013, "Estimation of Maximum Pullout Shear Stress of Grouted Soil Nails Using Bayesian Probabilistic Approach," *Int. J. Geomech.*, Vol. 13, No. 5, pp. 659–664, https://doi.org/10.1061/(ASCE)GM.1943-5622.0000259